K2-99: a subgiant hosting a transiting warm Jupiter in an eccentric orbit and a long-period companion

Smith, A.M.S.; Gandolfi, D.; Barragán, O.; Bowler, B.; Csizmadia, S.; Endl, M.; ... ; Wolthoff, V.

Monthly Notices of the ROYAL ASTRONOMICAL SOCIETY

MNRAS **464,** 2708–2716 (2017) doi:10.1093/mnras/stw2487
Advance Access publication 2016 September 30

K2-99: a subgiant hosting a transiting warm Jupiter in an eccentric orbit and a long-period companion

A. M. S. Smith,[1]★ D. Gandolfi,[2,3] O. Barragán,[2] B. Bowler,[4]† Sz. Csizmadia,[1] M. Endl,[4] M. C. V. Fridlund,[5,6] S. Grziwa,[7] E. Guenther,[8] A. P. Hatzes,[8] G. Nowak,[9,10] S. Albrecht,[11] R. Alonso,[9,10] J. Cabrera,[1] W. D. Cochran,[4] H. J. Deeg,[9,10] F. Cusano,[12] Ph. Eigmüller,[1] A. Erikson,[1] D. Hidalgo,[9,10] T. Hirano,[13] M. C. Johnson,[4,14] J. Korth,[7] A. Mann,[4] N. Narita,[15,16,17] D. Nespral,[9,10] E. Palle,[9,10] M. Pätzold,[7] J. Prieto-Arranz,[9,10] H. Rauer,[1,18] I. Ribas,[19] B. Tingley[11] and V. Wolthoff[3]

[1]*Institute of Planetary Research, German Aerospace Center, Rutherfordstrasse 2, D-12489 Berlin, Germany*
[2]*Dipartimento di Fisica, Universitá di Torino, via P. Giuria 1, I-10125 Torino, Italy*
[3]*Landessternwarte Königstuhl, Zentrum für Astronomie der Universität Heidelberg, Königstuhl 12, D-69117 Heidelberg, Germany*
[4]*Department of Astronomy and McDonald Observatory, University of Texas at Austin, 2515 Speedway, Stop C1400, Austin, TX 78712, USA*
[5]*Leiden Observatory, University of Leiden, PO Box 9513, NL-2300 RA, Leiden, the Netherlands*
[6]*Department of Earth and Space Sciences, Chalmers University of Technology, Onsala Space Observatory, SE-439 92 Onsala, Sweden*
[7]*Rheinisches Institut für Umweltforschung, Abt. Planetenforschung, an der Universität zu Köln, Aachener Strasse 209, D-50931 Köln, Germany*
[8]*Thüringer Landessternwarte Tautenburg, Sternwarte 5, D-07778 Tautenburg, Germany*
[9]*Instituto de Astrofísica de Canarias, E-38205 La Laguna, Tenerife, Spain*
[10]*Departamento de Astrofísica, Universidad de La Laguna, E-38206 La Laguna, Tenerife, Spain*
[11]*Stellar Astrophysics Centre, Department of Physics and Astronomy, Aarhus University, Ny Munkegade 120, DK-8000 Aarhus C, Denmark*
[12]*INAF – Osservatorio Astronomico di Bologna, Via Ranzani 1, I-40127 Bologna, Italy*
[13]*Department of Earth and Planetary Sciences, Tokyo Institute of Technology, 2-12-1 Ookayama, Meguro-ku, Tokyo 152-8551, Japan*
[14]*Department of Astronomy, The Ohio State University, 140 West 18th Ave., Columbus, OH 43210, USA*
[15]*Department of Astronomy, The University of Tokyo, 7-3-1 Hongo, Bunkyo-ku, Tokyo 113-0033, Japan*
[16]*Astrobiology Center, National Institutes of Natural Sciences, 2-21-1 Osawa, Mitaka, Tokyo 181-8588, Japan*
[17]*National Astronomical Observatory of Japan, 2-21-1 Osawa, Mitaka, Tokyo 181-8588, Japan*
[18]*Center for Astronomy and Astrophysics, TU Berlin, Hardenbergstr 36, D-10623 Berlin, Germany*
[19]*Institut de Ciències de l'Espai (CSIC-IEEC), Carrer de Can Magrans, Campus UAB, E-08193 Bellaterra, Spain*

Accepted 2016 September 28. Received 2016 September 23; in original form 2016 September 1

ABSTRACT

We report the discovery from *K2* of a transiting planet in an 18.25-d, eccentric (0.19 ± 0.04) orbit around K2-99, an 11th magnitude subgiant in Virgo. We confirm the planetary nature of the companion with radial velocities, and determine that the star is a metal-rich ([Fe/H] = 0.20 ± 0.05) subgiant, with mass $1.60^{+0.14}_{-0.10}$ $M_{\odot}$ and radius 3.1 ± 0.1 $R_{\odot}$. The planet has a mass of 0.97 ± 0.09 M_{Jup} and a radius 1.29 ± 0.05 R_{Jup}. A measured systemic radial acceleration of $-2.12 \pm 0.04\,ms^{-1}\,d^{-1}$ offers compelling evidence for the existence of a third body in the system, perhaps a brown dwarf orbiting with a period of several hundred days.

Key words: planets and satellites: detection – planets and satellites: individual: K2-99 – planetary system.

1 INTRODUCTION

Exoplanets that transit their host star are vital for our understanding of planetary systems, not least because their sizes and – in combination with radial velocity (RV) measurements – their absolute masses can be measured. Recent results from the *CoRoT* (Moutou et al. 2013) and *Kepler* missions (Borucki et al. 2010) have both extended the parameter space of transiting planet discovery, particularly to longer orbital periods, and revolutionized our understanding of the planetary population of our Galaxy (e.g. Howard et al. 2012). A majority of the planets discovered by *Kepler*, however, orbit stars too faint to enable RV measurements, and other observations, such

★ E-mail: Alexis.Smith@dlr.de
† McDonald Prize Fellow.

as atmospheric characterization, to be performed. Despite the great successes of *Kepler*, most of the best-studied exoplanetary systems remain those discovered from the ground, by means of RV (in a few cases) or from surveys such as WASP (Pollacco et al. 2006) and HAT-net (Bakos et al. 2004).

The re-purposing of the *Kepler* satellite to observe a number of fields along the ecliptic plane, for ∼80 d each, the so-called *K2* mission (Howell et al. 2014), allows the gap between *Kepler* and the ground-based surveys to be bridged. *K2* observes a large number of relatively bright ($v \lesssim 12$) stars, and has discovered a significant number of planets around such stars (see Crossfield et al. 2016, for a summary of the discoveries from *K2*'s first few fields). *K2* also allows the detection of smaller, and longer period planets than are possible from the ground. The high-precision photometry achievable from space enables the discovery of small transit signals, and hence planets, as well as aiding the detection of long-period planets from just a few transits. The continuous nature of the observations eliminates the window functions associated with ground-based observations, and thus also helps to facilitate the discovery of relatively long-period systems.

K2's great strengths are its capability of finding both bright planetary systems and relatively long-period planets (at least by comparison with those discovered from the ground). The planetary system described in this paper, K2-99, is a prime example of a system that is both bright ($v = 11.15$) and long-period ($P = 18.25$ d). To date, only a handful of planets with periods longer than 10 d have been discovered by means of transits observed from the ground, and none with a period longer than that of K2-99 b. K2-99 is one of a small number[1] of transiting planetary systems containing a planet on a long-period (>10 d) orbit around a bright ($v < 12$) star.

Furthermore, K2-99 b transits a star that is about to ascend the red-giant branch, and joins a small, but growing number of planets known to transit subgiant stars. In contrast to planets of solar-like stars, very little is known about planets of stars more massive than the Sun. This lack of knowledge is unfortunate, because theories of planet formation make very different predictions, whether such planets are rare or frequent (Kornet, Różyczka & Stepinski 2004; Laughlin, Bodenheimer & Adams 2004; Ida & Lin 2005; Boss 2006; Kennedy & Kenyon 2008; Alibert, Mordasini & Benz 2011; Hasegawa & Pudritz 2013). Thus, studies of the frequency of planets of stars more massive than the Sun are excellent tests of theories of planet formation. To date, most of the 156 known planet hosts more massive than 1.5 $M_\odot$ are giant stars. According to the statistical analysis of Johnson et al. (2010a,b), the frequency of massive planets increases with stellar mass. However, because all of the systems included in those analyses were detected by means of optical RV measurements, because their orbit distribution is different from that of solar-like stars, and because there is also a lack of multiple planets, there are still some doubts as to whether the planets of giant stars are real (Sato et al. 2008; Lillo-Box, Barrado & Correia 2016). It is therefore necessary to confirm at least a few planets of stars more massive than the Sun by other methods. An important confirmation was the RV measurements in the near-IR recently carried out by Trifonov et al. (2015). The results for giant stars have furthermore been criticized in the sense that the masses of the giant stars could be wrong (Lloyd 2013; Schlaufman & Winn 2013).

[1] About a dozen according to the Exoplanet Data Explorer (Wright et al. 2011; http://www.exoplanets.org).

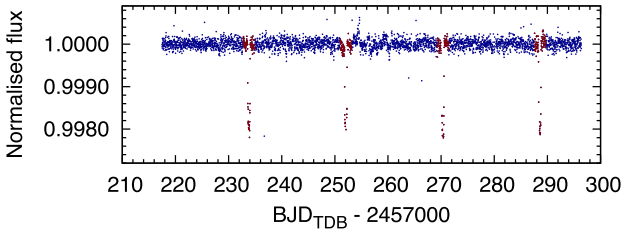

Figure 1. *K2* light curve of K2-99, processed by the K2SC code of Aigrain et al. (2016), which removes both instrumental and stellar noise. Portions of the light curve selected for modelling are shown in red (Section 3).

The best confirmation would therefore be the detection of transiting planets of giant, or subgiant stars that are more massive than 1.5 $M_\odot$, or of main sequence A-stars for which it is also certain that they are more massive 1.5 $M_\odot$. Up to now, 31 transiting planets of stars more massive than 1.5 $M_\odot$ have been detected, but most of them are main sequence F-stars. A dedicated survey for transiting planets of A-stars with the *CoRoT* satellite turned up one planet around an F-star, and six A-star host candidates. The number of candidates corresponds to the expectations if the frequency of massive, close-in planets of A-stars were the same as that of G-stars (Guenther et al. 2016). However, confirming these candidates is difficult given that the stars are faint, and rapidly rotating.

Only four planets are known to transit giant stars, and a further three transiting planets are known around subgiants (Section 4.1). It is therefore of crucial importance to detect more transiting planets of giant, and subgiant stars with $M_* > 1.5\,M_\odot$, in order to find out whether planets, particularly short-period ones, of such star are rare, or abundant. Here, we present the discovery of a transiting planet around a subgiant of mass $1.60^{+0.14}_{-0.10}$ $M_\odot$.

2 OBSERVATIONS

2.1 *K2* photometry

K2's Campaign 6 observations were centred on $\alpha = 13^{\rm h}\,39^{\rm m}\,28^{\rm s}$ $\delta = -11^\circ\,17'\,43''$ (2000.0) and ran from 2015 July 14 to 2015 September 30, i.e. for 78 d. A total of 28 289 targets were observed in the standard 30-min long-cadence mode, as well as 84 in short-cadence mode, and some custom targets.

K2-99 was identified as a candidate transiting planetary system from a search of *K2* light curves extracted by Vanderburg & Johnson (2014) performed using the EXOTRANS pipeline along with the VARLET filter (Grziwa, Pätzold & Carone 2012; Grziwa & Pätzold 2016). Four transits, spaced every ∼18.25 d, are clearly visible in the light curve of K2-99 (Fig. 1). On the basis of this detection (and the lack of odd–even transit-depth variations, and the lack of a visible secondary eclipse), the system was selected for spectroscopic follow-up observations.

Independently, K2-99 was identified as a candidate by Pope, Parviainen & Aigrain (2016). Using the K2SC code of Aigrain, Parviainen & Pope (2016), which relies on Gaussian processes to correct simultaneously the light curve for *K2* pointing systematics and stellar variability, Pope et al. (2016) identified a total of 152 candidate transiting systems from *K2* Campaigns 5 and 6. The K2SC light curve of K2-99 is shown in Fig. 1, and is the light curve used

Table 1. RV measurements, uncertainties, and cross-correlation function bisector spans (BS) of K2-99.

BJD_{TDB} −2450000	RV (km s^{-1})	σ_{RV} (km s^{-1})	BS (km s^{-1})	Instrument
7479.624340	−2.697	0.013	+0.013	FIES
7492.520141	−2.581	0.008	−0.007	HARPS-N
7493.757674	+0.502	0.019	–	Tull
7494.804635	+0.467	0.016	–	Tull
7502.643805	−2.493	0.007	−0.031	HARPS-N
7503.531525	−2.601	0.014	−0.003	FIES
7511.732010	−2.602	0.004	−0.040	HARPS
7512.508450	−2.616	0.005	+0.007	HARPS-N
7512.634721	−2.622	0.004	−0.000	HARPS
7515.726524	−2.617	0.012	+0.054	HARPS
7516.569369	−2.598	0.006	−0.053	HARPS
7523.478018	−2.630	0.019	−0.025	FIES
7524.768623	+0.446	0.015	–	Tull
7532.518735	−2.645	0.006	−0.034	HARPS-N
7539.461243	−2.558	0.005	−0.019	HARPS-N
7542.699191	+0.477	0.008	–	Tull
7543.736409	+0.433	0.011	–	Tull
7545.696704	+0.416	0.021	–	Tull
7559.601582	−2.620	0.005	−0.023	HARPS
7561.581344	−2.649	0.005	−0.014	HARPS
7565.410818	−2.806	0.016	−0.030	FIES
7566.413167	−2.798	0.014	−0.000	FIES
7567.416731	−2.849	0.014	−0.008	FIES
7568.417452	−2.834	0.018	+0.030	FIES
7570.405863	−2.819	0.016	−0.020	FIES
7572.408029	−2.809	0.016	−0.018	FIES
7575.409114	−2.740	0.018	−0.014	FIES
7576.403828	−2.726	0.015	+0.003	FIES
7577.404365	−2.757	0.020	+0.007	FIES
7578.405228	−2.761	0.016	+0.004	FIES
7579.402440	−2.807	0.022	+0.021	FIES
7589.495744	−2.779	0.006	−0.050	HARPS
7610.468090	−2.770	0.005	−0.025	HARPS

in the rest of this work, as it appears to be marginally less noisy than that of Vanderburg & Johnson (2014).[2]

2.2 Spectroscopic observations

In order to confirm the planetary nature of the transiting object and measure its mass, we performed intensive spectroscopic follow-up with the following spectrographs: FIES (Frandsen & Lindberg 1999; Telting et al. 2014), mounted on the 2.56-m Nordic Optical Telescope (NOT), and HARPS-N (Cosentino et al. 2012), mounted on the 3.58-m Telescopio Nazionale Galileo (TNG), both located at the Observatorio del Roque de los Muchachos, La Palma, Spain; HARPS (Mayor et al. 2003), on the ESO 3.6-m Telescope at La Silla, Chile; and the Robert G. Tull coudé spectrograph (Tull et al. 1995) on the 2.7-m Harlan J. Smith Telescope at McDonald Observatory, Texas, USA. The resulting RV measurements are listed in Table 1.

[2] After submission of this paper, we became aware of EVEREST (Luger et al. 2016), a *K2* de-trending algorithm that produces a light curve with slightly less noise still.

2.2.1 *FIES*

We acquired 14 FIES spectra between 2016 March and July. The instrument was used in its *high-res* mode, which provides a resolving power of $R \approx 67\,000$ in the spectral range 364–736 nm. We followed the same observing strategy adopted by Buchhave et al. (2010) and Gandolfi et al. (2015), i.e. we traced the RV drift of the instrument by acquiring long-exposed ($T_{exp} \approx 35$ s) ThAr spectra immediately before and after each target observation. The exposure times were 2700–3600 s, leading to a signal-to-noise ratio (S/N) of about 40–50 per pixel at 550 nm. The data were reduced using standard IRAF and IDL routines. RV measurements were derived via S/N-weighted, multi-order cross-correlations with the RV standard star HD 50692 – observed with the same instrument set-up as K2-99.

2.2.2 *HARPS-N*

We acquired five HARPS-N high-resolution spectra ($R \approx 115\,000$) between 2016 April and May, as part of the observing programmes A33TAC_11, A33TAC_15, and AOT33-11. We set the exposure time to 1800–2100 s and monitored the sky background using the second fibre. The data were reduced using the dedicated HARPS-N data reduction software pipeline. The S/N of the extracted spectra is about 40–50 per pixel at 550 nm. RVs (Table 1) were extracted by cross-correlation with a G2 numerical mask.

2.2.3 *HARPS*

We also acquired 11 HARPS high-resolution spectra ($R \approx 115\,000$) between 2016 April and August under the ESO programme 097.C-0948. We set the exposure time to 1800–2100 s, leading to a S/N of about 30–50 per pixel at 550 nm on the extracted spectra. We monitored the sky background using the second fibre and reduced the data with the HARPS data reduction software pipeline. RVs (Table 1) were extracted by cross-correlation with a G2 numerical mask. Three out of the 11 HARPS RVs are affected by technical problems and are not listed in Table 1. Nevertheless, the three HARPS spectra were used to derive the spectral parameters of K2-99, as described in Section 3.1.

2.2.4 *Tull*

We obtained six precise RV measurements with the Tull Coudé spectrograph. The instrument covers the entire optical spectrum at a resolving power of $R \approx 60\,000$. We used a molecular iodine (I_2) absorption cell for simultaneous wavelength calibration and point-spread function reconstruction. The differential RVs were calculated with our standard I_2-cell data modelling code AUSTRAL (Endl, Kürster & Els 2000). For the stellar template, we employed the co-added HARPS-N spectrum of K2-99 which has a sufficient high S/N of ∼100.

2.3 Imaging

In order to see if there exist close neighbours to K2-99 which could be diluting the transit signal, we performed adaptive-optics (AO) imaging of the target. We used the facility infrared imager NIRC2 at Keck Observatory using natural guide star AO (Wizinowich 2013) on 2016 July 15 UT. The narrow camera mode and K_S-band filter were chosen to finely sample the point-spread function with a high Strehl ratio. The resulting field of view was 10.2 arcsec × 10.2 arcsec. We acquired a set of 10 short, unsaturated frames

(10 co-adds × 0.1 s each) and five deeper frames (1 co-add × 60 s each) behind the partly opaque 600 mas diameter coronagraph mask. Images were bias subtracted, flat fielded, and corrected for bad pixels and cosmic rays. K2-99 appears single down to the diffraction limit [full width at half-maximum (FWHM) = 46.3 ± 1.2 mas] and no point sources are evident in the deeper images.

3 ANALYSIS

3.1 Spectral analysis

We separately co-added the FIES, HARPS, and HARPS-N data to produce three master spectra that were used to derive the stellar parameters of K2-99. We fitted the three master spectra to a grid of theoretical models from Castelli & Kurucz (2004), using spectral features that are sensitive to different photospheric parameters. We adopted the calibration equations for dwarf stars from Bruntt et al. (2010) and Doyle et al. (2014) to determine the microturbulent, $v_{\rm micro}$, and macroturbulent, $v_{\rm macro}$, velocities, respectively. The projected rotational velocity, $v \sin i_*$, was measured by fitting the profile of several unblended metal lines. We also used the spectral analysis package SME (version 4.43) to perform an independent spectral analysis. SME calculates synthetic spectra of stars and fits them to observed high-resolution spectra (Valenti & Piskunov 1996; Valenti & Fischer 2005). It solves for the model atmosphere parameters using a non-linear least squares algorithm. The two analyses provided consistent results well within the error bars regardless of the used spectrum. The final adopted values are reported in Table 2.

3.2 Joint analysis of photometry and radial velocities

The photometry and RVs were analysed simultaneously using the current version of the Transit Light Curve Modelling (TLCM) code (Csizmadia et al. 2015, in preparation). In brief, TLCM uses the Mandel & Agol (2002) model to fit the transit photometry, whilst simultaneously fitting a Keplerian orbit to the RVs. A genetic algorithm is used to optimize the fit, and then a simulated annealing chain uses the output of the genetic algorithm as a starting point, and estimates the uncertainties over a large number of steps (typically $\sim 10^5$). The Keplerian RV model is superimposed with a linear trend of RV with time (see Section 3.6); we also fitted for an offset in RV between FIES and each of the other spectrographs.

The light curve of K2-99 we model is that generated by the K2SC code of Aigrain et al. (2016) (see Section 2.1). We used only a subset of the light curve for modelling, selecting just over 1.5 times the transit duration both before and after each transit, such that the modelled light curve consists of four blocks of data, each around 2.2 d in duration, centred on each transit mid-point (see Fig. 1). This has the effect of reducing the number of photometric data points from 3516 to 372. Because the effective *K2* exposure time is relatively long (1800 s), we subdivide each exposure during the modelling, using a five-point Simpson integration.

The free parameters during the fitting process were the orbital period (P); the epoch of mid-transit ($T_{\rm c}$); the orbital major semi-axis in units of the stellar radius (a/R_*); the ratio of the planetary and stellar radii ($R_{\rm p}/R_*$); the orbital inclination angle ($i_{\rm p}$); the limb-darkening parameters, $u_+ = u_a + u_b$, and $u_- = u_a - u_b$, where u_a and u_b are the coefficients in a quadratic limb-darkening model; $e \sin\omega$ and $e \cos\omega$, where e is the orbital eccentricity, and ω is the argument of periastron; the systemic RV (γ); the stellar orbital velocity semi-amplitude (K); as well as the aforementioned radial acceleration ($\dot{\gamma}$) and instrumental RV offsets (γ_{2-1}, γ_{3-1}, and γ_{4-1}).

Table 2. Stellar parameters from our spectral analysis, and catalogue magnitudes for K2-99. References: Tycho: Høg et al. (2000). 2MASS: Skrutskie et al. (2006). WISE: Cutri et al. (2013).

Parameter	Value
RA (J2000.0)	$13^{\rm h}55^{\rm m}05\overset{\rm s}{.}7$
Dec. (J2000.0)	$-05^\circ26'32\overset{''}{.}88$
$T_{*,\rm eff}$	5990 ± 40 K
$\log g_*$ (cgs)	3.47 ± 0.06
$v_{\rm micro}$	1.2 ± 0.1 km s^{-1}
$v_{\rm macro}$	5.8 ± 0.6 km s^{-1}
$v \sin i_*$	9.3 ± 0.5 km s^{-1}
Spectral type	G0 IV
[Fe/H]	0.20 ± 0.05
[Ca/H]	0.30 ± 0.05
[Mg/H]	0.25 ± 0.05
Magnitudes	(from EPIC[a])
B (Tycho)	11.750 ± 0.113
g	11.332 ± 0.060
v (Tycho)	11.149 ± 0.099
r	10.957 ± 0.030
Kep	11.014
i	10.878 ± 0.040
J (2MASS)	10.024 ± 0.022
H (2MASS)	9.755 ± 0.021
K (2MASS)	9.720 ± 0.021
WISE 3.4 μm	9.685 ± 0.021
WISE 4.6 μm	9.714 ± 0.020
WISE 12 μm	9.721 ± 0.047
WISE 22 μm	8.850
Additional identifiers for K2-99:	
TYC 4974-871-1	
2MASS J13550570-0526330	

[a] *K2*'s Ecliptic Plane Input Catalog.

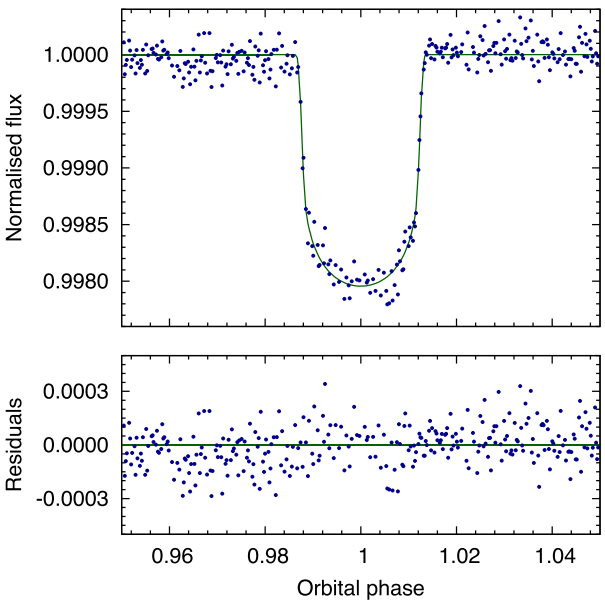

Figure 2. Phased light curve, overplotted with our best-fitting model.

The resulting fits to the transit photometry and the RVs are shown in Figs 2 and 3, respectively.

The stellar mass and radius were calculated by comparing the mean stellar density, the stellar effective temperature, and the

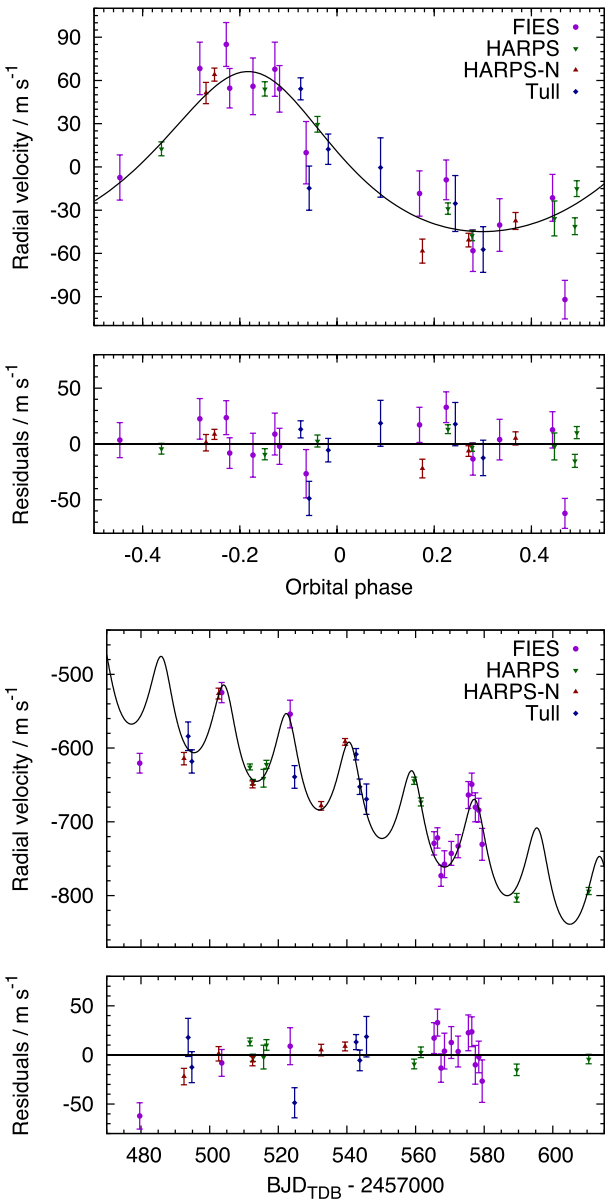

Figure 3. RVs as a function of orbital phase (upper panels) and time (lower panels), with best-fitting models and residuals to those models plotted below. Data points (with 1σ error bars) are from four different spectrographs, represented by different colours and symbol types.

stellar metallicity to theoretical isochrones. The stellar density was measured from the joint fitting of the transit light curve and the RVs (Table 3), and the stellar temperature and metallicity values are those derived in our spectral analysis (Section 3.1). We use the single star evolution (SSE) isochrones of Hurley, Pols & Tout (2000).

Calculating the planetary radius is then trivial, since R_p/R_* is known. The planet mass, M_p, is calculated according to

$$M_p \sin i = K \left(\frac{P}{2\pi G}\right)^{1/3} {M_*}^{2/3} \sqrt{1-e^2}, \quad (1)$$

given that $M_* \gg M_p$.

The stellar mass and radius calculated from isochrones can be used to calculate the logarithm of the stellar surface gravity, $\log g_* = 3.67 \pm 0.04$. This value is in reasonably good agreement with that computed from our spectral analysis (Section 3.1, Table 2). The stellar age was determined to be $2.4^{+0.2}_{-0.6}$ Gyr.

3.3 Orbital eccentricity

In addition to fitting for $e \sin\omega$ and $e \cos\omega$, when we found $e = 0.19 \pm 0.04$, we also tried fitting a circular orbit by fixing $e \sin\omega = e \cos\omega = 0$. Using the F-test approach of Lucy & Sweeney (1971), we find that there is a only a very small ($\approx 2 \times 10^{-4}$) probability that the apparent orbital eccentricity could have been observed if the underlying orbit were actually circular. We therefore conclude that the eccentricity we detect in the orbit of K2-99 b is significant.

3.4 Radial velocity bisectors and stellar activity

For the RV measurements obtained with FIES, HARPS, and HARPS-N, we were able to measure the BS. A correlation between the BS and RV is indicative of a blended eclipsing binary system, or of RV variation as a result of stellar activity (Queloz et al. 2001). As expected for a true planetary system, however, we see no significant correlation between the BS and RV (Fig. 4).

Furthermore, we observed no correlation between the RVs and either the corresponding FWHM values, or the $\log R'_{HK}$ activity index values (HARPS data only). The mean $\log R'_{HK}$ is -5.2 which, along with an apparent lack of photometric variability, is strongly suggestive of a relatively inactive star.

3.5 Reddening and stellar distance

We followed the method outlined in Gandolfi et al. (2008) to estimate the interstellar reddening (A_v) and distance d to the star. Briefly, A_v was derived by simultaneously fitting the observed colours (Table 2) with synthetic magnitudes computed from the NEXTGEN (Hauschildt, Allard & Baron 1999) model spectrum with the same spectroscopic parameter as K2-99. We assumed a normal value for the total-to-selective extinction [$R_v = A_v/E(B-v) = 3.1$] and adopted the interstellar extinction law of Cardelli, Clayton & Mathis (1989). The spectroscopic distance to the star was estimated using the de-reddened observed magnitudes and the NEXTGEN synthetic absolute magnitudes for a star with the same spectroscopic parameters and radius as K2-99. We found that $A_v = 0.05 \pm 0.05$ mag and $d = 606 \pm 32$ pc.

3.6 Evidence for a third body

3.6.1 Observed radial acceleration

We tried fitting the RVs both with and without the inclusion of a linear trend in time, finding that such a trend is heavily favoured by the data. Using the approach of Bowler (2016) (which follows Torres 1999 and Liu et al. 2002), we can place the following constraint on the properties of the third body, denoted by 'c':

$$\frac{M_c}{a_c^2} > 0.0145 \left|\frac{\dot{\gamma}}{\mathrm{m\ s^{-1}\ yr^{-1}}}\right| = 11\ \mathrm{M_{Jup}\ au^{-2}} \quad (2)$$

Furthermore, if we assume that the orbit of the third body is not significantly eccentric, we can infer that the period of the orbit must be at least twice the baseline of our RV data ($P_c > 236$ d). This leads to the constraints that $a_c \gtrsim 1.4$ au, and hence $M_c > 22\ \mathrm{M_{Jup}}$. The likeliest possibilities, then, are a brown dwarf orbiting within about 2.7 au; a $\sim \mathrm{M}_\odot$ object at $\sim$10 au; or an object orbiting on a

Table 3. System parameters from TLCM modelling.

Parameter	Symbol	Unit	Value
TLCM fitted parameters:			
Orbital period	P	d	18.249 ± 0.001
Epoch of mid-transit	T_c	BJD_{TDB}	2457233.823 ± 0.003
Scaled orbital major semi-axis	a/R_*	–	11.1 ± 0.1
Ratio of planetary to stellar radii	R_p/R_*	–	0.0422 ± 0.0006
Orbital inclination angle	i_p	$^\circ$	87.7 ± 0.3
–	$e \sin\omega$	–	0.03 ± 0.03
–	$e \cos\omega$	–	0.19 ± 0.04
Limb-darkening parameters	u_+	–	0.6 ± 0.1
	u_-	–	0.08 ± 0.20
Stellar orbital velocity semi-amplitude	K	$m\ s^{-1}$	56 ± 4
Systemic RV	γ	$km\ s^{-1}$	-2.08 ± 0.01
Systemic radial acceleration	$\dot{\gamma}$	$m\ s^{-1}\ d^{-1}$	-2.12 ± 0.04
Velocity offset between FIES and HARPS	γ_{2-1}	$m\ s^{-1}$	100 ± 8
Velocity offset between FIES and HARPS-N	γ_{3-1}	$m\ s^{-1}$	110 ± 7
Velocity offset between FIES and Tull	γ_{4-1}	$m\ s^{-1}$	316 ± 12
Derived parameters:			
Orbital eccentricity	e	...	0.19 ± 0.04
Argument of periastron	ω	$^\circ$	8 ± 8
Stellar mass	M_*	$M_\odot$	$1.60^{+0.14}_{-0.10}$
Stellar radius	R_*	$R_\odot$	3.1 ± 0.1
log (stellar surface gravity)	$\log g_*$	(cgs)	3.67 ± 0.04
Stellar density	ρ_*	$kg\ m^{-3}$	78 ± 3
Planet mass	M_p	M_{Jup}	0.97 ± 0.09
Planet radius	R_p	R_{Jup}	1.29 ± 0.05
log (planet surface gravity)	$\log g_p$	(cgs)	3.2 ± 0.1
Orbital major semi-axis	a	au	0.159 ± 0.006
Transit impact parameter	b	...	0.41 ± 0.05
Transit duration	T_{14}	d	0.50 ± 0.01
Stellar age	τ	Gyr	$2.4^{+0.2}_{-0.6}$
Distance (see Section 3.5)	d	pc	606 ± 32

highly eccentric orbit, such that we have just observed the portion of the orbit where the induced stellar RV is greatest.

Noting that the RV model described above does not fit the very first RV point well, we decided to fit the RVs using the RVLIN code and associated uncertainty estimator (Wright & Howard 2009; Wang et al. 2012). The parameters we obtained for a one-planet fit with a constant radial acceleration are in excellent agreement with those obtained using TLCM (Section 3.2). We then used RVLIN to fit a second planet to the RVs, instead of a radial acceleration term. Unsurprisingly, the fit to the second planet is poorly constrained, but if we assume a circular orbit for the second planet, we find $P_c = 485 \pm 310$ d and the orbital velocity amplitude due to the third body, $K_c = 230 \pm 150\ m\ s^{-1}$ (Fig. 5). These values are used to calculate the minimum mass, $M_c \sin i_c = 14 \pm 9\ M_{Jup}$ and orbital major semi-axis, $a_c = 1.4 \pm 1.0$ au. The two-planet fit results in a significantly lower χ^2 than the linear acceleration model, and also a lower BIC (accounting for the increased number of free parameters in the two-planet model). We note, however, that favouring the two-planet model over the constant radial acceleration model relies heavily (but not entirely) on a single data point, our first RV measurement, and therefore caution against overinterpretation of the two-planet fit.

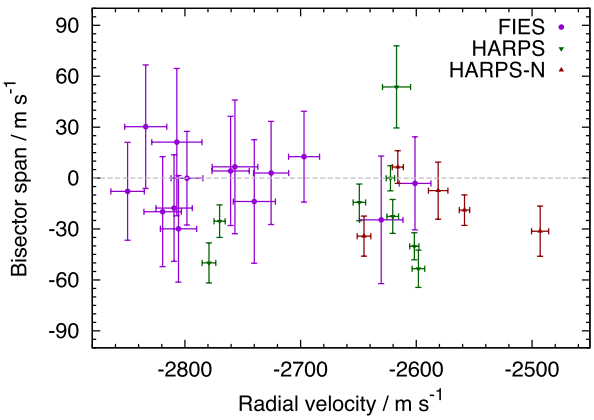

Figure 4. RV bisector span versus relative RV for data from the FIES, HARPS, and HARPS-N instruments. The uncertainties in the BS are taken to be twice the uncertainty in the RVs.

3.6.2 AO imaging

Contrast curves and sensitivity maps from our NIRC2 observations are generated in the same manner as described in Bowler et al. (2015). Unsaturated and coronagraphic images are first corrected for optical distortions using the distortion solution from Service et al. (2016); then the images were registered, de-rotated to a common position angle to account for slight rotation in pupil-tracking mode, median-combined, and north-aligned using the Service et al. (2016) north correction. 7σ contrast curves are generated using the rms in annuli centred on K2-99 together with the K_S-band coronagraph throughput measurement from (Bowler et al. 2015). Finally, sensitivity maps are derived by generating artificial companions on random circular orbits and comparing their

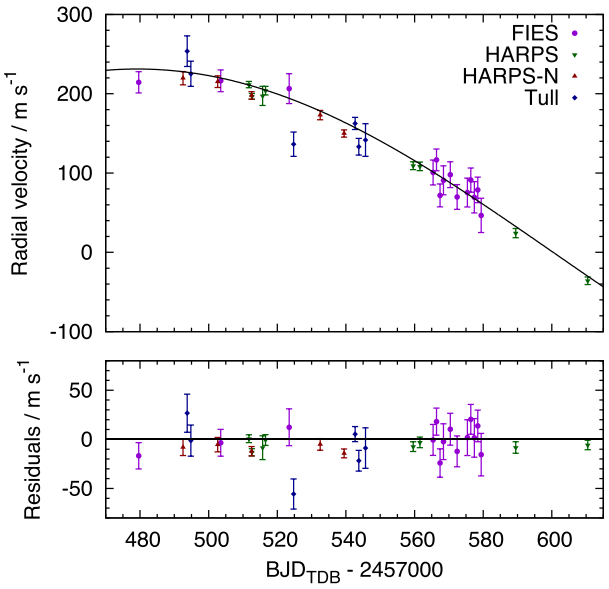

Figure 5. Residuals to the RV fit for K2-99 b, overplotted with a second fitted Keplerian orbit ($e = 0$, $P_c = 485 \pm 310$ d, $K_c = 230 \pm 150\,\mathrm{m\,s^{-1}}$). See Section 3.6.1 for details. The residuals to the double-Keplerian fit are plotted in the lower panel.

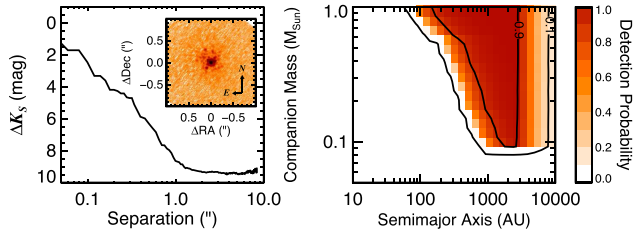

Figure 6. Detection limits for a luminous third body from NIRC2 imaging. The left-hand panel shows the contrast curve generated by combining our shallow unsaturated images (inset) with the deeper coronagraphic images. The right-hand panel shows the associated sensitivity to luminous third bodies (see Section 3.6.2 for details).

apparent magnitudes at the distance and age of K2-99 based on the evolutionary models of Baraffe et al. (2015) to our contrast curve. We also account for the fractional field of view coverage from the finite NIRC2 square detector. The resulting detection limits and sensitivity map are shown in Fig. 6.

Unfortunately, given the large distance to K2-99 (606 ± 32 pc), the only limits we can place on the presence of a third body from AO imaging are at rather large distances from the star ($\gtrsim$100 au). Both the observed radial acceleration and the second fitted Keplerian orbit (Section 3.6.1), however, suggest that the third body is closer to K2-99 than that. The radial acceleration alone suggests that a star orbiting at 100 au would need to be very massive ($\approx$100 $M_\odot$) to fit the observations. In other words, the AO imaging does not help us to distinguish between the various possible scenarios identified in Section 3.6.1.

3.7 Other effects visible in the light curve

We conducted searches for, and placed upper limits on various photometric effects besides the planetary transits:

Table 4. Fitted times of mid-transit for individual transits of K2-99, their uncertainties, and the deviation from the ephemeris presented in Table 3.

No.	$T_c - 2450000$ (BJD_{TDB})	σ_{T_c} (d)	O−C (d)
1	7233.8252	0.0015	+0.0017
2	7252.0708	0.0012	−0.0020
3	7270.3223	0.0010	+0.0001
4	7288.5722	0.0015	+0.0007

3.7.1 *Transit timing variations (TTV)*

We fitted for the epoch of each transit individually, using TLCM to fit only the part of the light curve corresponding to a single transit, and keeping all parameters fixed to their best-fitting values (Table 3), except for T_c that was allowed to vary. The individual times of mid-transit are reported in Table 4, and we see no evidence for any TTV. This non-detection is consistent with a maximum predicted TTV of 55 s, calculated from equation 32 of Borkovits et al. (2011), using the third body parameters from Section 3.6.1 and further assuming that the mutual inclination angle between the two orbital planes is zero. We also see no compelling evidence of transit depth or profile variations, such as those caused by star-spot crossing events.

3.7.2 *Planetary occultation and phase variation*

We tried fitting for an occultation (secondary eclipse), and determine a best-fitting depth of 22 ± 192 ppm, we therefore place an upper limit (95 per cent confidence) on the occultation depth of 405 ppm. Similarly, we see no evidence for any orbital phase variation.

3.7.3 *Stellar rotational modulation*

We searched for evidence of stellar rotational modulation using PERIOD04 (Lenz & Breger 2005). We used the light curve of Vanderburg & Johnson (2014), since stellar variability is removed by the K2SC pipeline. We found no evidence of such variability above an amplitude of 2×10^{-5} (95 per cent confidence limit).

3.7.4 *Additional transits*

We searched the light curve for additional transits using the DST code of Cabrera et al. (2012), but found no significant peaks in the periodogram which could indicate the existence of an additional transiting body.

4 DISCUSSION AND CONCLUSIONS

4.1 K2-99 as a subgiant planet host star

K2-99 joins a relatively short list of subgiants known to host transiting planets. The evolutionary tracks used to determine the stellar mass, radius, and age (Section 3.2; Hurley et al. 2000) suggest that the planet will be engulfed in around 150 Myr, as K2-99 expands further.

There have been several recent discoveries of transiting planets around subgiants, namely the short-period KELT-11b (Pepper et al. 2016, $P = 4.7$ d) and K2-39b (Van Eylen et al. 2016, $P = 4.6$ d), which also shows evidence for a long-period companion. K2-99 is most reminiscent, however, of the Kepler-435 system (=KOI-680;

Almenara et al. 2015), which consists of an F9 subgiant ($R_* = 3.2 \pm 0.3$) orbited by a giant planet in a slightly eccentric ($e = 0.11 \pm 0.08$) 8.6-d orbit. Kepler-435 also exhibits a radial acceleration, most likely due to a planetary mass object in a $P > 790$ d orbit.

4.2 K2-99 b as a warm Jupiter

Huang, Wu & Triaud (2016) note that there appears to be a distinction between hot ($P < 10$ d) and warm ($10 < P < 200$ d) Jupiters in that the latter are much more likely to have sub-Jovian companion planets. They find that around half of warm Jupiters (WJs) have smaller companions orbiting close to them, whereas this is true for only WASP-47 (Hellier et al. 2012; Becker et al. 2015) amongst the hot Jupiters. We find no evidence for the existence of any sub-Jovian companions to K2-99 although we note that we are less sensitive to small planets (because of the large stellar radius) and long-period planets (because of *K2*'s limited observing baseline) than the *Kepler* systems analysed by Huang et al. (2016). K2-99 also fits the correlation observed by Dawson & Murray-Clay (2013) that the orbits of WJs around metal-rich stars ([Fe/H] ≥ 0, like K2-99) have a range of eccentricities, whereas metal-poor stars host only planets on low-eccentricity orbits.

4.3 Possible migration scenarios for K2-99 b

Using equation (1) of Jackson, Greenberg & Barnes (2008), the current stellar parameters, and assuming a to be constant, we calculate the circularization time-scale, $\tau_e = \left(\frac{1}{e}\frac{\mathrm{d}e}{\mathrm{d}t}\right)^{-1}$, for the orbit of K2-99 b, in terms of the tidal dissipation parameters for the planet, Q_P, and for the star, Q_*,

$$\tau_e = \left(\frac{0.0104}{\left(\frac{Q_\mathrm{P}}{10^{5.5}}\right)} + \frac{0.0015}{\left(\frac{Q_*}{10^{6.5}}\right)}\right)^{-1} \mathrm{Gyr}, \quad (3)$$

Adopting $Q_\mathrm{P} = 10^{5.5}$ and $Q_* = 10^{6.5}$ (the best-fitting values from the study of Jackson et al. 2008), we find $\tau_e = 84$ Gyr. Even in the case that $Q_\mathrm{P} = 35\,000$ (the value for Jupiter; Lainey et al. 2009), and the extreme case that $Q_* = 10^5$, the circularization time-scale is still as long as 7.1 Gyr. These ages are much larger than the age of the system ($2.4^{+0.2}_{-0.6}$ Gyr), suggesting that the orbital eccentricity we observe is unlikely to have been significantly reduced by tidal interactions between the planet and star.

Dong, Katz & Socrates (2014) note that a greater fraction of eccentric warm Jupiter systems contain a third body capable of having caused the inward migration of the WJ via a high-eccentricity mechanism. Although the orbital eccentricity of K2-99 b is less than the threshold of 0.4 used by Dong et al. (2014) to demarcate high-eccentricity systems, the system does contain such a potential perturber. WJs with observed eccentricities less than 0.4, however, may merely be at a low-e stage in the cycle, and their orbits may become highly eccentric over a secular time-scale. If K2-99 b has undergone migration via a high-eccentricity route, such as Kozai migration, then one would expect the axis of its orbit to be significantly inclined with respect to the stellar spin axis (for it to have a large obliquity angle). We predict that the Rossiter–McLaughlin (R-M) effect for this system will have an amplitude of $\sim$11 m s^{-1}. Given that, and the $v \sin i_*$ of 9.3 ± 0.5 km s^{-1}, it should be possible to detect the R-M effect, and measure the sky-projected obliquity for this system. To date, only seven WJs ($P > 10$ d, $R_\mathrm{p} > 0.6\,R_\mathrm{Jup}$) have measured sky-projected obliquities, four of which are aligned and three of which show significant misalignment.[3] Further, Petrovich & Tremaine (2016) predict that the companions to WJs should have high mutual inclination angles than those of hot Jupiters, typically 60°–80°.

ACKNOWLEDGEMENTS

We wish to thank Trent Dupuy (University of Texas) for performing the AO observations. This paper includes data collected by the Kepler mission. Funding for the Kepler mission is provided by the NASA Science Mission directorate. Some of the data presented in this paper were obtained from the Mikulski Archive for Space Telescopes (MAST). STScI is operated by the Association of Universities for Research in Astronomy, Inc., under NASA contract NAS5-26555. Support for MAST for non-HST data is provided by the NASA Office of Space Science via grant NNX09AF08G and by other grants and contracts. SC acknowledges the Hungarian OTKA Grant K113117. NN acknowledges a support by Grant-in-Aid for Scientific Research (A) (JSPS KAKENHI Grant Number 25247026). We are very grateful to the NOT, ESO, TNG, and McDonald staff members for their unique support during the observations. We are also very thankful to Jorge Melendez, Martin Kürster, Nuno Santos, Xavier Bonfils, and Tsevi Mazeh who kindly agreed to exchange HARPS and FIES time with us. Based on observations obtained (a) with the NOT, operated on the island of La Palma jointly by Denmark, Finland, Iceland, Norway, and Sweden, in the Spanish Observatorio del Roque de los Muchachos (ORM) of the Instituto de Astrofísica de Canarias (IAC); (b) with the Italian TNG also operated at the ORM (IAC) on the island of La Palma by the INAF – Fundación Galileo Galilei. Based on observations made with ESO Telescopes at the La Silla Observatory under programme ID 097.C-0948. This paper includes data taken at McDonald Observatory of the University of Texas at Austin. The research leading to these results has received funding from the European Union Seventh Framework Programme (FP7/2013-2016) under grant agreement No. 312430 (OPTICON) and from the NASA K2 Guest Observer Cycle 1 program under grant NNX15AV58G to The University of Texas at Austin. This research has made use of NASA's Astrophysics Data System, the SIMBAD data base, operated at CDS, Strasbourg, France, the Exoplanet Orbit Database and the Exoplanet Data Explorer at exoplanets.org, the Exoplanets Encyclopaedia at exoplanet.eu, and René Heller's Holt–Rossiter–McLaughlin Encyclopaedia (http://www.astro.physik.uni-goettingen.de/~rheller). We thank the anonymous referee for comments which helped to improve this manuscript.

REFERENCES

Aigrain S., Parviainen H., Pope B. J. S., 2016, MNRAS, 459, 2408
Alibert Y., Mordasini C., Benz W., 2011, A&A, 526, A63
Almenara J. M. et al., 2015, A&A, 575, A71
Bakos G., Noyes R. W., Kovács G., Stanek K. Z., Sasselov D. D., Domsa I., 2004, PASP, 116, 266
Baraffe I., Homeier D., Allard F., Chabrier G., 2015, A&A, 577, A42
Becker J. C., Vanderburg A., Adams F. C., Rappaport S. A., Schwengeler H. M., 2015, ApJ, 812, L18

[3] Statistics are from René Heller's Holt–Rossiter–McLaughlin Encyclopaedia, accessed on 2016 August 17 (http://www.astro.physik.uni-goettingen.de/~rheller).

Borkovits T., Csizmadia S., Forgács-Dajka E., Hegedüs T., 2011, A&A, 528, A53
Borucki W. J. et al., 2010, Science, 327, 977
Boss A. P., 2006, ApJ, 644, L79
Bowler B. P., 2016, PASP, 128, 102001
Bowler B. P., Liu M. C., Shkolnik E. L., Tamura M., 2015, ApJS, 216, 7
Bruntt H. et al., 2010, MNRAS, 405, 1907
Buchhave L. A. et al., 2010, ApJ, 720, 1118
Cabrera J., Csizmadia S., Erikson A., Rauer H., Kirste S., 2012, A&A, 548, A44
Cardelli J. A., Clayton G. C., Mathis J. S., 1989, ApJ, 345, 245
Castelli F., Kurucz R. L., 2004, preprint (arXiv:0405087)
Cosentino R. et al., 2012, in Proc. SPIE Conf. Ser. Vol. 8446, Ground-based and Airborne Instrumentation for Astronomy IV. SPIE, Bellingham, p. 84461V
Crossfield I. J. M. et al., 2016, ApJS, 226, 7
Csizmadia S. et al., 2015, A&A, 584, A13
Cutri R. M. et al., 2013, VizieR Online Data Catalog, 2328
Dawson R. I., Murray-Clay R. A., 2013, ApJ, 767, L24
Dong S., Katz B., Socrates A., 2014, ApJ, 781, L5
Doyle A. P., Davies G. R., Smalley B., Chaplin W. J., Elsworth Y., 2014, MNRAS, 444, 3592
Endl M., Kürster M., Els S., 2000, A&A, 362, 585
Frandsen S., Lindberg B., 1999, in Karttunen H., Piirola V., eds, Astrophysics with the NOT. Univ. Turku, Tuorla Observatory, Piikkio, Finland, p. 71
Gandolfi D. et al., 2008, ApJ, 687, 1303
Gandolfi D. et al., 2015, A&A, 576, A11
Grziwa S., Pätzold M., 2016, MNRAS, preprint (arXiv:1607.08417)
Grziwa S., Pätzold M., Carone L., 2012, MNRAS, 420, 1045
Guenther E. W. et al., 2016, The CoRoT Legacy Book: The Adventure of the Ultra High Precision Photometry from Space. EDP Science, p. 149
Hasegawa Y., Pudritz R. E., 2013, ApJ, 778, 78
Hauschildt P. H., Allard F., Baron E., 1999, ApJ, 512, 377
Hellier C. et al., 2012, MNRAS, 426, 739
Howard A. W. et al., 2012, ApJS, 201, 15
Howell S. B. et al., 2014, PASP, 126, 398
Huang C., Wu Y., Triaud A. H. M. J., 2016, ApJ, 825, 98
Hurley J. R., Pols O. R., Tout C. A., 2000, MNRAS, 315, 543
Høg E. et al., 2000, A&A, 355, L27
Ida S., Lin D. N. C., 2005, ApJ, 626, 1045
Jackson B., Greenberg R., Barnes R., 2008, ApJ, 678, 1396
Johnson J. A., Howard A. W., Bowler B. P., Henry G. W., Marcy G. W., Wright J. T., Fischer D. A., Isaacson H., 2010a, PASP, 122, 701
Johnson J. A. et al., 2010b, ApJ, 721, L153
Kennedy G. M., Kenyon S. J., 2008, ApJ, 673, 502
Kornet K., Różyczka M., Stepinski T. F., 2004, A&A, 417, 151
Lainey V., Arlot J.-E., Karatekin Ö., van Hoolst T., 2009, Nature, 459, 957
Laughlin G., Bodenheimer P., Adams F. C., 2004, ApJ, 612, L73
Lenz P., Breger M., 2005, Commun. Asteroseismol., 146, 53
Lillo-Box J., Barrado D., Correia A. C. M., 2016, A&A, 589, A124
Liu M. C., Fischer D. A., Graham J. R., Lloyd J. P., Marcy G. W., Butler R. P., 2002, ApJ, 571, 519
Lloyd J. P., 2013, ApJ, 774, L2
Lucy L. B., Sweeney M. A., 1971, AJ, 76, 544
Luger R., Agol E., Kruse E., Barnes R., Becker A., Foreman-Mackey D., Deming D., 2016, AJ, 152, 100
Mandel K., Agol E., 2002, ApJ, 580, L171
Mayor M. et al., 2003, The Messenger, 114, 20
Moutou C. et al., 2013, Icarus, 226, 1625
Pepper J. et al., 2016, preprint (arXiv:1607.01755)
Petrovich C., Tremaine S., 2016, ApJ, 829, 132
Pollacco D. L. et al., 2006, PASP, 118, 1407
Pope B. J. S., Parviainen H., Aigrain S., 2016, MNRAS, 461, 3399
Queloz D. et al., 2001, A&A, 379, 279
Sato B. et al., 2008, in Fischer D., Rasio F. A., Thorsett S. E., Wolszczan A., eds, ASP Conf. Ser. Vol. 398, Extreme Solar Systems. Astron. Soc. Pac., San Francisco, p. 67
Schlaufman K. C., Winn J. N., 2013, ApJ, 772, 143
Service M., Lu J. R., Campbell R., Sitarski B. N., Ghez A. M., Anderson J., 2016, PASP, 128, 095004
Skrutskie M. F. et al., 2006, AJ, 131, 1163
Telting J. H. et al., 2014, Astron. Nachr., 335, 41
Torres G., 1999, PASP, 111, 169
Trifonov T., Reffert S., Zechmeister M., Reiners A., Quirrenbach A., 2015, A&A, 582, A54
Tull R. G., MacQueen P. J., Sneden C., Lambert D. L., 1995, PASP, 107, 251
Valenti J. A., Fischer D. A., 2005, ApJS, 159, 141
Valenti J. A., Piskunov N., 1996, A&AS, 118, 595
Van Eylen V. et al., 2016, AJ, preprint (arXiv:1605.09180)
Vanderburg A., Johnson J. A., 2014, PASP, 126, 948
Wang Sharon X. et al., 2012, ApJ, 761, 46
Wizinowich P., 2013, PASP, 125, 798
Wright J. T., Howard A. W., 2009, ApJS, 182, 205
Wright J. T. et al., 2011, PASP, 123, 412

This paper has been typeset from a TEX/LATEX file prepared by the author.